axioms

MDPI

Article

Finite-Difference Schemes for Interval Advection Equations Within a New Interval-Calculus Framework

Jiahui Wang [1], Guoju Ye [1], Wei Liu [1], Abdul Mateen [2,*] and Ghada AlNemer [3]

1 School of Mathematics, Hohai University, Nanjing 210098, China
2 School of Mathematics and Statistics, Shandong Normal University, Jinan 250358, China
3 Department of Mathematical Sciences, College of Science, Princess Nourah bint Abdulrahman University, Riyadh 11671, Saudi Arabia
* Correspondence: aabdulmateen1996@gmail.com

Abstract

This paper focuses on three finite difference schemes for the interval advection equation based on a novel interval calculus framework. Different from classical interval arithmetic, this innovative framework equips the interval number space with a rigorous Hilbert space structure and enables a critical decoupling of the derivative for interval-valued functions, where the center component obeys classical differentiation rules and the radius component complies with multiplicative differentiation principles. Using this unique decoupling property, we construct interval counterparts of three representative classical finite difference schemes, namely the Upwind, Lax–Friedrichs, and Lax–Wendroff schemes, and conduct a comprehensive and rigorous theoretical assessment of their numerical properties. Utilizing the inherent isometric isomorphism between the interval space and $\mathbb{R}^2$, we rigorously establish the consistency of the proposed schemes and adopt the von Neumann method for systematic stability analysis. A sharp, explicit Courant–Friedrichs–Lewy (CFL) condition is derived, which jointly accounts for the center velocity and logarithmic radius velocity of the interval advection field, and the scheme convergence is strictly guaranteed via the Lax equivalence theorem. Extensive numerical experiments are carried out to validate the theoretical conclusions and verify the practical merits of the developed interval schemes. The numerical results demonstrate that the proposed methods retain nearly constant interval width in long-duration simulations, completely bypass the switching-point complexity that intrinsically exists in traditional generalized Hukuhara (gH)-based interval approaches, and deliver competitive computational efficiency. This work corroborates that the newly proposed interval calculus framework serves as an elegant, solid, and versatile foundation for the numerical computation and analysis of interval partial differential equations.

Keywords: interval analysis; new interval calculus; advection equation; finite difference methods; multiplicative calculus

MSC: 35R13; 65M06; 65M12

Check for updates

Academic Editor: Mingji Zhang

Received: 23 July 2026
Revised: 16 August 2026
Accepted: 19 August 2026
Published: 21 August 2026

Copyright: © 2026 by the authors. Licensee MDPI, Basel, Switzerland. This article is an open access article distributed under the terms and conditions of the Creative Commons Attribution (CC BY) license.

1. Introduction

Interval analysis, since its formal inception by Moore [1], has served as a fundamental mathematical framework for handling uncertainty in computational mathematics. By representing uncertain quantities as closed intervals rather than precise real numbers, interval methods have found widespread applications in areas ranging from numerical optimization [2] and differential equations [3,4] to engineering design [5] and, more recently, machine learning [6]. The core advantage of interval computation lies in its ability to provide rigorous enclosures that guarantee the containment of true solutions, thereby offering a reliable tool for uncertainty quantification.

Despite its conceptual appeal, classical interval arithmetic, often referred to as Moore arithmetic, suffers from significant algebraic deficiencies. The space of interval numbers under the conventional operations $\oplus$ and $\ominus$ forms only a semi-linear space; in particular, subtraction is not the inverse of addition, leading to the well-known phenomenon of *interval overestimation* or artificial width growth during long computations. To mitigate some of these issues, the generalized Hukuhara derivative (gH-derivative) was introduced by Stefanini and Bede [3] and has since become a standard tool in interval differential equations. Nevertheless, the gH-derivative requires a case-by-case inspection of *switching points* where the interval endpoints cross, which complicates both the theoretical analysis and the numerical implementation of interval partial differential equations (PDEs).

Recently, Liu, Ali, and An [7] proposed a *new interval calculus* that fundamentally restructures interval arithmetic. In this new framework, the space of interval numbers $\mathbb{R}_{\mathcal{I}}$ forms a strict linear space. In particular, it constitutes a Hilbert space equipped with a natural norm and inner product. Moreover, the interval derivative admits a clean decomposition into a classical derivative for the center of the interval and a multiplicative derivative for its radius. This decoupling eliminates the need for switching-point tracking and provides a transparent algebraic structure that is ideally suited for the construction and analysis of numerical schemes for interval PDEs.

Multiplicative calculus itself has attracted increasing attention as an alternative to Newtonian calculus. Introduced by Grossman and Katz [8] and rigorously developed by Bashirov, Kurpinar, and Özyapici [9], multiplicative differentiation replaces the roles of subtraction and addition with division and multiplication. It has proven particularly effective for modeling phenomena characterized by exponential growth or proportional scaling. In the context of numerical methods for PDEs, Yazici and Selvitopi [10] developed finite difference algorithms for the multiplicative heat equation, while Cubillos [11] demonstrated that multiplicative schemes can circumvent the minimum-points-per-wavelength sampling constraints for wave propagation problems. Foundational work on multiplicative finite difference methods was carried out by Riza, Özyapici, and Misirli [12], and further developed for multiplicative Runge–Kutta schemes by Aniszewska [13] and for multiplicative Adams–Bashforth–Moulton methods by Misirli and Gurefe [14]. However, to the best of our knowledge, the combination of the new interval calculus with multiplicative numerical techniques for the solution of interval advection equations has not been explored in the literature.

The purpose of this paper is to bridge this gap. We develop, analyze, and numerically validate a family of finite difference schemes for the interval advection equation within the new interval calculus framework. Specifically, the main contributions of this work are threefold:

(1) We construct interval analogues of the classical Upwind, Lax–Friedrichs, and Lax–Wendroff schemes directly in the interval space $\mathbb{R}_{\mathcal{I}}$. Each scheme is presented both in a compact interval form and in a component-wise multiplicative form, where the radius update follows a multiplicative advection equation, cleanly separated from the classical advection of the center.

(2) We provide a rigorous theoretical analysis of the proposed schemes. Using the isometric isomorphism between $\mathbb{R}_{\mathcal{I}}$ and $\mathbb{R}^2$, we prove consistency and derive the corresponding CFL stability condition $\max(|a_c|, |\ln a_w|)\Delta t/\Delta x \leq 1$, where a_c and a_w denote the center and radius of the interval advection velocity. Convergence is then established via the Lax equivalence theorem.

(3) Through a series of numerical experiments, we demonstrate that the new interval schemes completely avoid the artificial width growth and switching-point complexity inherent in traditional gH-based methods [1,3]. The computational efficiency and robustness of the proposed schemes are validated, highlighting their practical advantages for long-time simulations of uncertain advection processes.

The remainder of this paper is organized as follows. Section 2 reviews the necessary concepts from the new interval calculus and multiplicative differentiation. In Section 3, we formulate the interval advection equation and derive its decoupled center-radius form with periodic boundary conditions. Section 4 is devoted to the construction of the interval Upwind, Lax–Friedrichs, and Lax–Wendroff schemes in both interval and component-wise forms. The theoretical analysis of consistency, stability, and convergence is presented in Section 5. Section 6 reports the numerical experiments, including comparisons with the gH-Upwind scheme, that corroborate the theoretical findings. Finally, Section 7 concludes the paper and outlines directions for future research.

2. Preliminaries

In this section, we briefly review the essential concepts of the new interval calculus introduced by Liu et al. [7] and the multiplicative calculus developed by Bashirov et al. [9].

2.1. Multiplicative Calculus

The multiplicative calculus, introduced by Grossman and Katz [8] and rigorously developed by Bashirov et al. [9], provides an alternative to the classical Newtonian calculus by replacing the roles of subtraction and addition with division and multiplication. This calculus is particularly effective for modeling phenomena characterized by exponential growth or proportional scaling, and it plays a central role in the decoupling of the interval advection equation.

Definition 1 (Multiplicative derivative)**.** *Let $f : (a, b) \to (0, \infty)$ be a positive function. The multiplicative derivative of f at x is*

$$f^*(x) = \lim_{h\to 0}\left(\frac{f(x+h)}{f(x)}\right)^{1/h} = e^{(\ln f)'(x)}. \tag{1}$$

If $f^*(x)$ exists, then f is said to be multiplicatively differentiable at x.

Higher-order multiplicative derivatives are defined inductively. If the n-th classical derivative of $\ln f$ exists, then the n-th multiplicative derivative of f exists and is given by

$$f^{*(n)}(x) = e^{(\ln f)^{(n)}(x)}, \qquad n = 0, 1, 2, \ldots, \tag{2}$$

where $f^{*(0)} = f$. In particular, the second multiplicative derivative is $f^{**}(x) = e^{(\ln f)''(x)}$.

Proposition 1. *Let f and g be multiplicatively differentiable, let h be differentiable, and let c be a positive constant. Then*

- $(cf)^*(x) = f^*(x)$;
- $(fg)^*(x) = f^*(x)g^*(x)$;
- $(f/g)^*(x) = f^*(x)/g^*(x)$;
- $(f^h)^*(x) = f^*(x)^{h(x)} \cdot f(x)^{h'(x)}$.

Theorem 1 (Multiplicative Taylor theorem)**.** *Let f be $(n+1)$ times multiplicatively differentiable on an open interval containing x. Then for any $x+h$ in that interval, there exists $\theta \in (0,1)$ such that*

$$f(x+h) = f(x) \cdot \prod_{m=1}^{n} \left(f^{*(m)}(x)\right)^{\frac{h^m}{m!}} \cdot \left(f^{*(n+1)}(x+\theta h)\right)^{\frac{h^{n+1}}{(n+1)!}}. \tag{3}$$

For the construction of the Lax–Wendroff scheme in Section 4, the first three terms of the expansion will be particularly useful:

$$f(x \pm h) = f(x) \cdot \left[f^{*}(x)\right]^{\pm h} \cdot \left[f^{**}(x)\right]^{\frac{h^2}{2}} \cdot \left[f^{*(3)}(x)\right]^{\pm \frac{h^3}{6}} \cdots\cdot. \tag{4}$$

2.2. The Interval Space $\mathbb{R}_{\mathcal{I}}$

Let $\mathbb{R}$ be the set of real numbers. An *interval number* $\overline{a}$ is a closed and bounded interval $[a_l, a_r]$ with $a_l < a_r$. We exclusively use the *center-radius representation*

$$\overline{a} = \langle a_c; a_w \rangle, \qquad a_c = \frac{a_l + a_r}{2}, \quad a_w = \frac{a_r - a_l}{2} > 0. \tag{5}$$

The set of all such interval numbers is denoted by $\mathbb{R}_{\mathcal{I}}$.

The new interval arithmetic equips $\mathbb{R}_{\mathcal{I}}$ with a genuine linear structure. The fundamental arithmetic operations are defined as follows.

Definition 2 (Interval arithmetic operations, [7])**.** *For $\overline{a} = \langle a_c; a_w \rangle$, $\overline{b} = \langle b_c; b_w \rangle \in \mathbb{R}_{\mathcal{I}}$ and $k \in \mathbb{R}$, we define the following:*

- ***Addition:*** $\overline{a} + \overline{b} = \langle a_c + b_c;\ a_w b_w \rangle$;
- ***Subtraction:*** $\overline{a} - \overline{b} = \left\langle a_c - b_c;\ \dfrac{a_w}{b_w} \right\rangle$;
- ***Scalar multiplication:*** $k\overline{a} = \langle k a_c;\ a_w^k \rangle$;
- ***Interval multiplication:*** $\overline{a} \times \overline{b} = \langle a_c b_c;\ e^{\ln a_w \ln b_w} \rangle$.

Remark 1. *To avoid conceptual confusion in the center-radius representation, we distinguish four fundamental notions:*

(1) Additive identity (zero element): $\bar{0} = \langle 0; 1 \rangle$. In interval addition, the radius component is multiplied, so 1 acts as its identity.

(2) Multiplicative identity (unit element): $\bar{1} = \langle 1; e \rangle$. Neutral for interval multiplication because $\ln e = 1$.

(3) Stationary logarithmic-radius speed: $\ln a_w = 0$ i.e., $a_w = 1$, means the interval radius remains unchanged under advection.

(4) Geometric half-width: a_w itself is the physical radius, quantifying the absolute uncertainty magnitude.

Thus, $a_w = 1$ characterizes stationary uncertainty, not a point interval. A point interval with zero uncertainty is $\bar{u} = \langle u_c; 1 \rangle$. A key feature of this arithmetic is that subtraction is the exact inverse of addition: $\bar{a} - \bar{a} = \bar{0}$, which prevents artificial interval width growth. Classical Moore arithmetic does not possess this property.

To highlight the distinctiveness of the new framework, we juxtapose it with the *generalized Hukuhara difference* (gH-difference) introduced by Stefanini and Bede [3], a standard tool in traditional interval analysis. For intervals in endpoint form $[a_l, a_r]$, the gH-difference is defined as

$$\overline{a} \ominus_{gH} \overline{b} = \left[\min\{a_l - b_l,\ a_r - b_r\},\ \max\{a_l - b_l,\ a_r - b_r\}\right]. \tag{6}$$

In center-radius notation, this is equivalent to

$$\overline{a} \ominus_{gH} \overline{b} = \langle a_c - b_c;\ |a_w - b_w| \rangle. \tag{7}$$

Note that the gH-difference involves the absolute value of the difference of the radii, which is the source of the switching-point complexity that plagues traditional interval schemes. This should be contrasted with the new interval subtraction, where the radius operation is a simple division, completely eliminating the need for case-by-case endpoint tracking.

The interval space $\mathbb{R}_{\mathcal{I}}$ is equipped with the following inner product and induced norm.

Definition 3 (Interval inner product and norm, [7])**.** *For $\overline{a} = \langle a_c; a_w \rangle, \overline{b} = \langle b_c; b_w \rangle \in \mathbb{R}_{\mathcal{I}}$,*

$$\overline{a} \circ \overline{b} = a_c b_c + \ln a_w \ln b_w, \qquad \|\overline{a}\| = \sqrt{\overline{a} \circ \overline{a}} = \sqrt{a_c^2 + (\ln a_w)^2}. \tag{8}$$

Theorem 2. *The space $\mathbb{R}_{\mathcal{I}}$ endowed with the inner product $\circ$ is a real Hilbert space. In particular, the mapping $\Phi : \mathbb{R}_{\mathcal{I}} \to \mathbb{R}^2$ defined by $\Phi(\langle a_c; a_w \rangle) = (a_c, \ln a_w)$ is an isometric isomorphism (see Liu et al. [7]).*

This isometric isomorphism is the cornerstone of our theoretical analysis in Section 5, as it allows us to transfer convergence and stability proofs directly from the classical Euclidean setting.

2.3. Interval-Valued Functions and Their Derivatives

An *interval-valued function* (IVF) is a mapping $\overline{f} : [a, b] \to \mathbb{R}_{\mathcal{I}}$. Every such function can be uniquely represented by its center and radius functions,

$$\overline{f}(x) = \langle f_c(x); f_w(x) \rangle, \quad x \in [a, b], \tag{9}$$

where $f_c, f_w : [a, b] \to \mathbb{R}$ and $f_w(x) > 0$.

Definition 4 (Interval derivative, [7])**.** *An IVF $\overline{f}$ is differentiable at $x_0 \in [a, b]$ if the limit*

$$\overline{f}'(x_0) = \lim_{h \to 0} \frac{\overline{f}(x_0 + h) - \overline{f}(x_0)}{h} \tag{10}$$

exists in $\mathbb{R}_{\mathcal{I}}$, where the subtraction is interpreted in the sense of the new interval arithmetic.

Theorem 3 (Interval derivative decomposition, [7])**.** *Let $\overline{f}(x) = \langle f_c(x); f_w(x) \rangle$ be an IVF. Then $\overline{f}$ is differentiable at x if and only if f_c is differentiable in the classical sense and f_w is differentiable in the multiplicative sense. Moreover,*

$$\overline{f}'(x) = \langle f_c'(x); f_w^*(x) \rangle. \tag{11}$$

For a bivariate IVF $\bar{u}(x, t) = \langle u_c(x, t); u_w(x, t) \rangle$, the partial derivatives decompose componentwise. Taking the spatial derivative as an illustrative example,

$$\bar{u}_x = \frac{\partial \bar{u}}{\partial x} = \left\langle \frac{\partial u_c}{\partial x};\ u_w \frac{\partial (\ln u_w)}{\partial x} \right\rangle = \langle (u_c)_x;\ (u_w)_x^* \rangle,$$

where $(u_w)_x^* = u_w (\ln u_w)_x$ denotes the multiplicative partial derivative of the uncertainty radius. The time derivative obeys the identical decomposition. We thus adopt the compact notation

$$\overline{u}_t = \langle (u_c)_t; (u_w)_t^* \rangle, \qquad \overline{u}_x = \langle (u_c)_x; (u_w)_x^* \rangle. \tag{12}$$

This decomposition is the theoretical foundation for the decoupling of the interval advection equation in Section 3.

3. The Interval Advection Equation in $\mathbb{R}_{\mathcal{I}}$

In this section, we formulate the interval advection equation within the framework of the new interval calculus introduced by Liu et al. [7]. We then derive a fundamental decoupling property that reduces the interval-valued partial differential equation to a pair of independent classical advection equations. This decomposition serves as the theoretical foundation for the numerical schemes developed in Section 4.

3.1. Problem Statement

We consider the initial-boundary value problem for the interval advection equation on a bounded spatial domain with periodic boundary conditions:

$$\begin{cases} \overline{u}_t + \overline{a}\,\overline{u}_x = \overline{0}, & (x,t) \in [0,L] \times (0,T], \\ \overline{u}(0,t) = \overline{u}(L,t), & t \in [0,T], \\ \overline{u}(x,0) = \overline{u}_0(x), & x \in [0,L], \end{cases} \tag{13}$$

where $\overline{u}(x,t) = \langle u_c(x,t); u_w(x,t)\rangle$ is the unknown interval-valued function, and $\overline{a} = \langle a_c; a_w\rangle \in \mathbb{R}_{\mathcal{I}}$ is the interval advection velocity with $a_w > 0$. The initial datum is given in center-radius form as $\overline{u}_0(x) = \langle u_{c,0}(x); u_{w,0}(x)\rangle$. All arithmetic operations in (13) follow the new interval arithmetic described in Section 2, and the derivatives $\overline{u}_t$ and $\overline{u}_x$ are interpreted in the sense of Definition 4.

The periodic boundary condition in (13) is the standard choice for analyzing finite difference schemes for linear advection equations. It eliminates boundary-induced complications while preserving the essential features of wave propagation and enables the use of von Neumann stability analysis in Section 5. The extension to other boundary conditions, such as inflow/outflow or Dirichlet, follows by applying the corresponding classical treatment to each decoupled component separately.

3.2. Decoupling via Center-Radius Representation

We now exploit the decomposition property of the new interval calculus to reduce (13) to a pair of classical advection equations.

Let the unknown function and the advection velocity be written in center-radius coordinates as $\overline{u}(x,t) = \langle u_c(x,t); u_w(x,t)\rangle$ and $\overline{a} = \langle a_c; a_w\rangle$. By Theorem 3, the partial derivatives are

$$\overline{u}_t = \langle (u_c)_t; (u_w)^*_t\rangle, \qquad \overline{u}_x = \langle (u_c)_x; (u_w)^*_x\rangle. \tag{14}$$

The advection term $\overline{a}\,\overline{u}_x$ involves the multiplication of two interval numbers. Applying the interval multiplication rule from Section 2, we obtain

$$\overline{a}\,\overline{u}_x = \langle a_c; a_w\rangle \times \langle (u_c)_x; (u_w)^*_x\rangle = \langle a_c(u_c)_x; e^{\ln a_w \cdot \ln((u_w)^*_x)}\rangle. \tag{15}$$

Using the interval addition rule, the complete equation becomes

$$\overline{u}_t + \overline{a}\,\overline{u}_x = \langle (u_c)_t + a_c(u_c)_x;\ (u_w)^*_t \cdot e^{\ln a_w \cdot \ln((u_w)^*_x)}\rangle. \tag{16}$$

Equating this to the zero element $\overline{0} = \langle 0; 1\rangle$ and taking the natural logarithm of the radius component using the identity $\ln f^* = (\ln f)'$, we arrive at the following decoupled system of classical linear advection equations:

$$\begin{aligned}(u_c)_t + a_c(u_c)_x &= 0,\\ (\ln u_w)_t + (\ln a_w)(\ln u_w)_x &= 0.\end{aligned} \tag{17}$$

The initial condition $\overline{u}(x,0) = \langle u_{c,0}(x); u_{w,0}(x)\rangle$ provides the corresponding initial data

$$u_c(x,0) = u_{c,0}(x), \qquad \ln u_w(x,0) = \ln u_{w,0}(x), \qquad x \in [0,L]. \tag{18}$$

The periodic boundary condition in (13) translates directly to periodic boundary conditions for each decoupled component:

$$u_c(0,t) = u_c(L,t), \qquad \ln u_w(0,t) = \ln u_w(L,t), \qquad t \in [0,T]. \tag{19}$$

The decoupled system (17)–(19) reveals several important structural properties of the interval advection equation under the new interval calculus.

(1) **Independent propagation of center and radius.** The center function u_c propagates with velocity a_c, while the logarithm of the radius function $\ln u_w$ propagates with velocity $\ln a_w$. Notably, the two velocities are completely independent. This feature stems directly from the multiplicative nature of interval arithmetic. In traditional interval analysis (e.g., using Moore's arithmetic or the gH-derivative), the evolution of the interval endpoints is typically coupled and may require tracking switching points [3]. Here, the center-radius representation together with the new operations yields a clean separation of dynamics.

(2) **Physical interpretation of uncertainty propagation.** The center u_c represents the most probable value of the transported quantity, whereas the radius u_w quantifies the uncertainty spread around it. In the decoupled system (17), the two velocities play distinct physical roles:

- The center velocity a_c governs the deterministic advection speed of the interval's position, i.e., the rate at which the most probable value propagates through the domain. This is the classical advection speed familiar from deterministic PDEs.
- The logarithmic radius velocity $\ln a_w$ governs the propagation speed of the magnitude of uncertainty. If $\ln a_w > 0$, the interval width grows exponentially along the characteristic, reflecting uncertainty amplification; if $\ln a_w < 0$, it decays, indicating uncertainty contraction. The special case $\ln a_w = 0$ (i.e., $a_w = 1$) corresponds to a stationary uncertainty width (see Remark 1 for details), where the interval radius remains constant during advection.

This transparent separation of position and spread provides a physically intuitive mechanism. This mechanism models input uncertainty encoded in $\bar{a}$. It captures the time-dependent evolution of this uncertainty. It sets the present framework apart from classical interval methods.

(3) **Absence of switching points.** Because the system (17) is fully decoupled, there is no need to inspect whether the left and right endpoints of the interval cross during the evolution. Endpoint crossing constitutes a notorious complication in gH-based schemes. This property will be shown in Section 6 to yield both computational efficiency and robustness.

(4) **Simplified boundary treatment.** The decoupling extends naturally to the boundary conditions: the periodic conditions (13) for the interval-valued problem reduce

to independent periodic conditions (19) for u_c and $\ln u_w$. Consequently, any well-established numerical boundary treatment for the classical advection equation can be applied separately to each component, without requiring special interval-valued boundary operators or switching-point logic at the boundaries. This principle extends to other boundary conditions (e.g., inflow/outflow, Dirichlet), which can be imposed component-wise.

Remark 2. *The decoupling (17) can also be understood through the lens of the isometric isomorphism $\Phi : \mathbb{R}_{\mathcal{I}} \to \mathbb{R}^2$ established in Theorem 2. Under the logarithmic mapping $\Phi(\langle a_c; a_w\rangle) = (a_c, \ln a_w)$, the interval advection Equation (13) is mapped to a diagonal system of two classical advection equations. This geometric perspective will be central to the convergence analysis in Section 5.*

4. Interval Difference Schemes

In this section, we construct three finite difference schemes for the interval advection Equation (13) within the new interval calculus framework. We adopt a uniform spatial grid $x_j = j\Delta x$ ($j = 0, 1, \ldots, M$) and temporal grid $t_n = n\Delta t$ ($n = 0, 1, \ldots, N$), where $\Delta x = L/M$ and $\Delta t = T/N$ are the spatial and temporal step sizes, respectively. The numerical approximation to $\overline{u}(x_j, t_n)$ is denoted by $\overline{U}_j^n = \langle (U_c)_j^n; (U_w)_j^n \rangle$. The mesh ratio is defined as $r = \Delta t/\Delta x$. Note that the multiplicative structure characterizes only the evolution of the uncertainty radius, whereas the spatial coordinate itself remains additive.

4.1. Construction of Interval Upwind Scheme

For the derivation below, we assume without loss of generality that $a_c > 0$ and $\ln a_w > 0$, so that the upwind direction is from the left. The formulas for arbitrary signs of the advection velocities can be obtained by adjusting the stencil accordingly, as in the classical case.

The classical first-order upwind scheme for the scalar advection equation $v_t + cv_x = 0$ (with $c > 0$) is

$$v_j^{n+1} = v_j^n - c\, r(v_j^n - v_{j-1}^n).$$

In the framework of the new interval calculus, we propose the interval Upwind scheme for (13):

$$\overline{U}_j^{n+1} = \overline{U}_j^n - \overline{a}\, r\Big(\overline{U}_j^n - \overline{U}_{j-1}^n\Big). \tag{20}$$

To reveal the underlying component-wise dynamics and to provide a practical formula for implementation, we expand (20) in terms of the center-radius representation. Using the arithmetic rules from Section 2, the interval difference is

$$\overline{D}_j^n = \overline{U}_j^n - \overline{U}_{j-1}^n = \left\langle (U_c)_j^n - (U_c)_{j-1}^n;\ \frac{(U_w)_j^n}{(U_w)_{j-1}^n} \right\rangle.$$

Applying the interval multiplication and scalar multiplication successively yields

$$r\,\overline{a}\,\overline{D}_j^n = \left\langle a_c r\Big((U_c)_j^n - (U_c)_{j-1}^n\Big);\ \exp\!\left(r \ln a_w \cdot \ln \frac{(U_w)_j^n}{(U_w)_{j-1}^n}\right) \right\rangle,$$

where $r = \Delta t/\Delta x$. Finally, the interval subtraction gives the component-wise form

$$\overline{U}_j^{n+1} = \langle (U_c)_j^{n+1}; (U_w)_j^{n+1} \rangle, \tag{21}$$

with the center and radius updated according to

$$
\begin{aligned}
(U_c)_j^{n+1} &= (U_c)_j^n - a_c r\Big((U_c)_j^n - (U_c)_{j-1}^n\Big),\\
(U_w)_j^{n+1} &= (U_w)_j^n \cdot \left(\frac{(U_w)_j^n}{(U_w)_{j-1}^n}\right)^{-\ln a_w \cdot r}.
\end{aligned}
\tag{22}
$$

Remark 3. *The radius update in* (22) *is written in a multiplicative form, which clearly exhibits the multiplicative advection nature: the new radius is obtained from the old one by multiplying by a power of the ratio of neighboring radii. By taking logarithms, one recovers the classical upwind scheme for* $\ln u_w$ *with advection velocity* $\ln a_w$*, consistent with the decoupled system* (17)*.*

4.2. Construction of Interval Lax–Friedrichs Scheme

The classical Lax–Friedrichs scheme for $v_t + cv_x = 0$ is

$$
v_j^{n+1} = \frac{1}{2}(v_{j+1}^n + v_{j-1}^n) - \frac{cr}{2}(v_{j+1}^n - v_{j-1}^n).
$$

Its interval counterpart is constructed analogously as the interval Lax–Friedrichs scheme:

$$
\overline{U}_j^{n+1} = \frac{1}{2}\Big(\overline{U}_{j+1}^n + \overline{U}_{j-1}^n\Big) - \overline{a}\,\frac{r}{2}\Big(\overline{U}_{j+1}^n - \overline{U}_{j-1}^n\Big). \tag{23}
$$

Expanding (23) into center-radius components, we compute the averaging term and the flux difference term separately. For the averaging term, scalar multiplication by $1/2$ yields

$$
\frac{1}{2}\Big(\overline{U}_{j+1}^n + \overline{U}_{j-1}^n\Big) = \left\langle \frac{1}{2}((U_c)_{j+1}^n + (U_c)_{j-1}^n);\ \sqrt{(U_w)_{j+1}^n (U_w)_{j-1}^n} \right\rangle.
$$

For the flux difference term, let $\overline{D} = \overline{U}_{j+1}^n - \overline{U}_{j-1}^n$ with

$$
D_c = (U_c)_{j+1}^n - (U_c)_{j-1}^n, \qquad D_w = \frac{(U_w)_{j+1}^n}{(U_w)_{j-1}^n}.
$$

Then $\overline{a}\,\overline{D} = \langle a_c D_c;\ e^{\ln a_w \ln D_w}\rangle$, and after scalar multiplication we obtain

$$
\frac{r}{2}\,\overline{a}\,\overline{D} = \left\langle \frac{a_c r}{2} D_c;\ \exp\!\left(\frac{r}{2}\ln a_w \cdot \ln\frac{(U_w)_{j+1}^n}{(U_w)_{j-1}^n}\right) \right\rangle.
$$

Performing the interval subtraction and simplifying the radius component using the properties of exponentials, we arrive at the following compact multiplicative form for the radius update:

$$
(U_w)_j^{n+1} = \sqrt{(U_w)_{j+1}^n (U_w)_{j-1}^n} \cdot \left(\frac{(U_w)_{j+1}^n}{(U_w)_{j-1}^n}\right)^{-\frac{r}{2}\ln a_w}. \tag{24}
$$

Thus, the complete component-wise form of the interval Lax–Friedrichs scheme reads

$$
\overline{U}_j^{n+1} = \langle (U_c)_j^{n+1}; (U_w)_j^{n+1} \rangle, \tag{25}
$$

with

$$
\begin{aligned}
(U_c)_j^{n+1} &= \frac{1}{2}\Big((U_c)_{j+1}^n + (U_c)_{j-1}^n\Big) - \frac{a_c r}{2}\Big((U_c)_{j+1}^n - (U_c)_{j-1}^n\Big),\\
(U_w)_j^{n+1} &= \sqrt{(U_w)_{j+1}^n (U_w)_{j-1}^n} \cdot \left(\frac{(U_w)_{j+1}^n}{(U_w)_{j-1}^n}\right)^{-\frac{r}{2}\ln a_w}.
\end{aligned}
\tag{26}
$$

Remark 4. *The multiplicative form* (26) *shows that the radius update is a geometric mean of the neighboring radii multiplied by a correction factor that captures the advective flux in the multiplicative sense. Taking the logarithm of* (24) *recovers the classical Lax–Friedrichs stencil for* $\ln u_w$ *with velocity* $\ln a_w$*, confirming consistency with* (17)*. The Lax–Friedrichs scheme is known to introduce numerical dissipation; in the interval context this will cause some smearing of the interval width over time, as will be observed in Section 6.*

4.3. Construction of Interval Lax–Wendroff Scheme

The Lax–Wendroff scheme is a second-order accurate method obtained by expanding the solution in a Taylor series and replacing time derivatives by spatial derivatives using the governing PDE. For the scalar advection equation, it takes the form

$$v_j^{n+1} = v_j^n - \frac{cr}{2}(v_{j+1}^n - v_{j-1}^n) + \frac{c^2r^2}{2}(v_{j+1}^n - 2v_j^n + v_{j-1}^n).$$

Following the same logic within the new interval calculus, we propose the interval Lax–Wendroff scheme:

$$\overline{U}_j^{n+1} = \overline{U}_j^n - \overline{a}\,\frac{r}{2}\Big(\overline{U}_{j+1}^n - \overline{U}_{j-1}^n\Big) + \frac{1}{2}\,\overline{a}^2 r^2\Big(\overline{U}_{j+1}^n - 2\overline{U}_j^n + \overline{U}_{j-1}^n\Big). \tag{27}$$

Here $\overline{a}^2 = \overline{a} \times \overline{a} = \langle a_c^2;\, e^{(\ln a_w)^2}\rangle$ by the interval multiplication rule. The second-order term $\overline{a}^2$ introduces the factor $(\ln a_w)^2$ in the radius component. Expanding (27) by the same procedure as above, we obtain the component-wise form

$$\overline{U}_j^{n+1} = \langle (U_c)_j^{n+1}; (U_w)_j^{n+1}\rangle, \tag{28}$$

where the center and radius are updated as

$$\begin{aligned} (U_c)_j^{n+1} &= (U_c)_j^n - \frac{a_c r}{2}\Big((U_c)_{j+1}^n - (U_c)_{j-1}^n\Big) \\ &\qquad + \frac{a_c^2 r^2}{2}\Big((U_c)_{j+1}^n - 2(U_c)_j^n + (U_c)_{j-1}^n\Big), \\ (U_w)_j^{n+1} &= (U_w)_j^n \cdot \left(\frac{(U_w)_{j+1}^n}{(U_w)_{j-1}^n}\right)^{-\frac{r}{2}\ln a_w} \cdot \left(\frac{(U_w)_{j+1}^n (U_w)_{j-1}^n}{((U_w)_j^n)^2}\right)^{\frac{r^2}{2}(\ln a_w)^2}. \end{aligned} \tag{29}$$

Remark 5. *The radius update in* (29) *is expressed entirely in multiplicative form, mirroring the structure of the classical Lax–Wendroff scheme but with geometric ratios and powers instead of differences and sums. By taking logarithms, one immediately verifies that* $\ln U_w$ *satisfies the classical Lax–Wendroff scheme with advection velocity* $\ln a_w$*. This guarantees that the interval Lax–Wendroff scheme is second-order accurate in both space and time, as will be proved in Section 5.*

Remark 6 (Boundary conditions)**.** *The schemes presented above are written for interior grid points. The periodic boundary condition* (13) *for the interval problem translates, via* (19)*, to periodic boundary conditions for both* U_c *and* $\ln U_w$ *at the discrete level. This allows a straightforward implementation using standard periodic index wrapping (e.g.,* $j-1 \mapsto M-1$ *when* $j=0$*, and* $j+1 \mapsto 0$ *when* $j = M-1$*) for each component independently. The extension to other boundary conditions follows by the same component-wise principle.*

5. Consistency, Stability, and Convergence Analysis

In this section, we establish the theoretical foundations of the interval finite difference schemes proposed in Section 4. The analysis is carried out directly in the interval space

$\mathbb{R}_{\mathcal{I}}$, using the norm and arithmetic operations introduced in Section 2. By exploiting the isometric isomorphism Φ between $\mathbb{R}_{\mathcal{I}}$ and $\mathbb{R}^2$, we prove the consistency and stability of the schemes. Convergence then follows from the Lax equivalence theorem for linear problems. Throughout this section, we assume that the spatial domain is equipped with periodic boundary conditions as stated in (13), which allows us to employ the classical von Neumann (Fourier) stability analysis on the interval grid functions.

5.1. Discrete Norm and Truncation Error

For a grid function $\overline{U}^n = \{\overline{U}_j^n\}$ defined on a uniform spatial mesh with step size Δx, the discrete L_2 norm induced by the interval norm $\|\cdot\|$ is

$$\|\overline{U}^n\|_{L_2} = \left(\Delta x \sum_j \|\overline{U}_j^n\|^2\right)^{1/2} = \left(\Delta x \sum_j \Big(((U_c)_j^n)^2 + (\ln(U_w)_j^n)^2\Big)\right)^{1/2}. \tag{30}$$

It follows from Equation (30) and the isometric isomorphism in Theorem 2 that this discrete L_2 interval norm is equivalent to the Euclidean norm of $(U_c, \ln U_w)$ with mesh-independent equivalence constants, which is an essential hypothesis for the Lax equivalence theorem.

Let $\overline{u}(x,t) = \langle u_c(x,t); u_w(x,t)\rangle$ be the exact solution of the interval advection Equation (13). For a given finite difference scheme written in the compact form $\overline{U}_j^{n+1} = \overline{\mathcal{H}}(\overline{U}^n)_j$, the local truncation error $\overline{\mathcal{T}}_j^n$ at the grid point (x_j, t_n) is an **interval-valued quantity** defined as the residual when the exact solution is substituted into the scheme, divided by the time step:

$$\overline{\mathcal{T}}_j^n = \frac{\overline{u}(x_j, t_{n+1}) - \overline{\mathcal{H}}(\overline{u}(\cdot, t_n))_j}{\Delta t}, \tag{31}$$

where the subtraction is in the sense of the new interval arithmetic (Definition 2). The scheme is said to be consistent if $\|\overline{\mathcal{T}}_j^n\| \to 0$ as $\Delta t, \Delta x \to 0$.

A key technical tool for the subsequent analysis is the isometric isomorphism $\Phi : \mathbb{R}_{\mathcal{I}} \to \mathbb{R}^2$ established in Theorem 2, which maps $\langle a_c; a_w\rangle \mapsto (a_c, \ln a_w)$. Under this mapping, the interval norm coincides with the Euclidean norm on $\mathbb{R}^2$, and the interval truncation error $\overline{\mathcal{T}}_j^n$ corresponds to the vector of classical truncation errors for the center and logarithmic radius components. This allows us to reduce the analysis of interval schemes to the well-understood analysis of classical finite difference methods.

Regularity assumptions. The exact solution $\bar{u}(x,t) = \langle u_c(x,t); u_w(x,t)\rangle$ satisfies the following smoothness conditions:

(1) For the Upwind scheme and the Lax–Friedrichs scheme:

$$u_c \in C^2([0,L] \times [0,T]), \qquad \ln u_w \in C^2([0,L] \times [0,T]),$$

which ensures that all Taylor expansions up to second order are valid and the remainder terms are uniformly bounded.

(2) For the Lax–Wendroff scheme, we require the stronger condition:

$$u_c \in C^4([0,L] \times [0,T]), \qquad \ln u_w \in C^4([0,L] \times [0,T]),$$

which is necessary to control the higher-order remainder terms in the fourth-order Taylor expansion used in the cancellation argument.

These assumptions are standard in the consistency analysis of finite difference methods for linear hyperbolic PDEs and guarantee that the local truncation errors are well-defined and bounded.

5.2. Consistency Analysis

We now establish the consistency of the three interval schemes. The proofs proceed by expressing the interval truncation error in terms of its center-radius components via the isomorphism Φ, applying classical Taylor expansion techniques to each component, and then reconstructing the interval norm estimate. The consistency analysis below is conducted under the regularity assumptions stated at the end of Section 5.1.

5.2.1. Interval Upwind Scheme

Lemma 1 (Consistency of the Interval Upwind Scheme)**.** *The interval Upwind scheme* (20) *is consistent with the interval advection Equation* (13)*. Moreover, under the fixed mesh ratio $\Delta t/\Delta x = \lambda$, its local truncation error satisfies*

$$\|\overline{\mathcal{T}}_j^n\| = O(\Delta t + \Delta x) \quad \textit{as} \quad \Delta t, \Delta x \to 0. \tag{32}$$

Proof. Substituting the exact solution into the interval Upwind scheme (20) and using the definition (31), we write the interval truncation error as

$$\overline{\mathcal{T}}_j^n = \frac{1}{\Delta t}\left(\overline{u}(x_j, t_{n+1}) - \left[\overline{u}(x_j, t_n) - \overline{a}\frac{\Delta t}{\Delta x}\big(\overline{u}(x_j, t_n) - \overline{u}(x_{j-1}, t_n)\big)\right]\right). \tag{33}$$

Applying the isometric isomorphism Φ to (33), the interval truncation error corresponds to the vector

$$\Phi(\overline{\mathcal{T}}_j^n) = \big((\mathcal{T}_c)_j^n, (\mathcal{T}_{\ln w})_j^n\big),$$

where $(\mathcal{T}_c)_j^n$ and $(\mathcal{T}_{\ln w})_j^n$ are the classical local truncation errors of the first-order upwind scheme applied to the advection equations for u_c (with velocity a_c) and $\ln u_w$ (with velocity $\ln a_w$), respectively.

We now analyze $(\mathcal{T}_c)_j^n$ in detail. Direct substitution of u_c into the center component of (22) yields

$$\begin{aligned}(\mathcal{T}_c)_j^n &= \frac{u_c(x_j, t_{n+1}) - u_c(x_j, t_n)}{\Delta t} + a_c\frac{u_c(x_j, t_n) - u_c(x_{j-1}, t_n)}{\Delta x} \\ &= \big((u_c)_t + a_c(u_c)_x\big)\big|_{(x_j,t_n)} + \frac{\Delta t}{2}(u_c)_{tt}\big|_{(x_j,\bar{t}_n)} - a_c\frac{\Delta x}{2}(u_c)_{xx}\big|_{(\bar{x}_j,t_n)},\end{aligned} \tag{34}$$

where $\bar{t}_n \in (t_n, t_{n+1})$ and $\bar{x}_j \in (x_{j-1}, x_j)$ are intermediate points obtained from the standard Taylor expansions

$$u_c(x_j, t_{n+1}) = u_c(x_j, t_n) + \Delta t (u_c)_t\big|_{(x_j,t_n)} + \frac{\Delta t^2}{2}(u_c)_{tt}\big|_{(x_j,\bar{t}_n)},$$

$$u_c(x_{j-1}, t_n) = u_c(x_j, t_n) - \Delta x (u_c)_x\big|_{(x_j,t_n)} + \frac{\Delta x^2}{2}(u_c)_{xx}\big|_{(\bar{x}_j,t_n)}.$$

Since u_c satisfies $(u_c)_t + a_c(u_c)_x = 0$ from the decoupled system (17), the leading term in (34) vanishes. Under the smoothness assumption $u_c \in C^2$, the second derivatives are bounded, yielding

$$|(\mathcal{T}_c)_j^n| = \left|\frac{\Delta t}{2}(u_c)_{tt} - a_c\frac{\Delta x}{2}(u_c)_{xx}\right| \le C_1(\Delta t + \Delta x),$$

for some constant $C_1 > 0$ independent of Δt and Δx.

Now analyze $(\mathcal{T}_{\ln w})_j^n$ in parallel. Let $v = \ln u_w$ and $b = \ln a_w$. Substituting the exact solution into the logarithmic-radius update yields

$$(\mathcal{T}_{\ln w})_j^n = \frac{v(x_j, t_{n+1}) - v(x_j, t_n)}{\Delta t} + b\frac{v(x_j, t_n) - v(x_{j-1}, t_n)}{\Delta x}$$
$$= (v_t + bv_x)|_{(x_j, t_n)} + \frac{\Delta t}{2} v_{tt}\Big|_{(x_j, \bar{t}_n)} - b\frac{\Delta x}{2} v_{xx}\Big|_{(\bar{x}_j, t_n)},$$

where $\bar{t}_n \in (t_n, t_{n+1})$ and $\bar{x}_j \in (x_{j-1}, x_j)$ are intermediate points from the Taylor expansions. Since v satisfies $v_t + bv_x = 0$ from the decoupled system (17), the leading term vanishes. Under the smoothness assumption $v \in C^2$, the second derivatives are bounded, giving

$$|(\mathcal{T}_{\ln w})_j^n| = \left| \frac{\Delta t}{2} v_{tt} - b\frac{\Delta x}{2} v_{xx} \right| \leq C_2(\Delta t + \Delta x),$$

for some constant $C_2 > 0$ independent of Δt and Δx.

Finally, by the isometric property of Φ,

$$\|\overline{\mathcal{T}}_j^n\| = \sqrt{|(\mathcal{T}_c)_j^n|^2 + |(\mathcal{T}_{\ln w})_j^n|^2} \leq \sqrt{C_1^2 + C_2^2}\,(\Delta t + \Delta x),$$

which establishes the estimate (32). □

Remark 7. *The interval Upwind scheme preserves the first-order accuracy of its classical counterpart. Its low dissipation makes it suitable for long-time simulations where the interval width must be maintained with minimal artificial smearing.*

5.2.2. Interval Lax–Friedrichs Scheme

Lemma 2 (Consistency of the Interval Lax–Friedrichs Scheme)**.** *The interval Lax–Friedrichs scheme* (23) *is consistent with the interval advection Equation* (13)*. Moreover, under the fixed mesh ratio* $\Delta t/\Delta x = \lambda$*, its local truncation error satisfies*

$$\|\overline{\mathcal{T}}_j^n\| = O(\Delta t + \Delta x) \quad \textit{as} \quad \Delta t, \Delta x \to 0. \tag{35}$$

Proof. The proof follows the same isometric isomorphism strategy as in Lemma 1. The component-wise form (26) shows that the center U_c and the logarithmic radius $\ln U_w$ are each advanced by the classical Lax–Friedrichs scheme with velocities a_c and $\ln a_w$, respectively.

We briefly sketch the classical analysis for completeness. For the classical Lax–Friedrichs scheme applied to a scalar advection equation $v_t + cv_x = 0$, substituting the exact solution and expanding via Taylor series yields

$$\mathcal{T}_{\text{LF}} = \frac{v(x_j, t_{n+1}) - \frac{1}{2}(v(x_{j+1}, t_n) + v(x_{j-1}, t_n))}{\Delta t} + c\frac{v(x_{j+1}, t_n) - v(x_{j-1}, t_n)}{2\Delta x}$$
$$= (v_t + cv_x)\big|_{(x_j, t_n)} + \frac{\Delta t}{2} v_{tt} - \frac{\Delta x^2}{2\Delta t} v_{xx} + O(\Delta t^2 + \Delta x^2)$$
$$= \frac{1}{2}\left(\Delta t\, v_{tt} - \frac{\Delta x^2}{\Delta t} v_{xx}\right) + O(\Delta t^2 + \Delta x^2), \tag{36}$$

where we used $v_t + cv_x = 0$ to eliminate the leading term. Under the fixed mesh ratio $\Delta t/\Delta x = \lambda$, the term $\Delta x^2/\Delta t = (1/\lambda)\Delta x$ is $O(\Delta x)$, and the dominant error is $O(\Delta t + \Delta x)$.

Applying the above expansion to the center component u_c with velocity a_c recovers the first-order truncation error $(\mathcal{T}_c)_j^n$. For the logarithmic-radius component $v = \ln u_w$ with velocity $b = \ln a_w$, the identical Taylor expansion gives

$$(\mathcal{T}_{\ln w})_j^n = \frac{1}{2}\left(\Delta t\, v_{tt} - \frac{\Delta x^2}{\Delta t} v_{xx}\right) + O(\Delta t^2 + \Delta x^2),$$

which is also first-order accurate under fixed mesh ratio. Combining the two component errors via the interval norm as in the previous proof, we obtain (35). □

Remark 8. *The Lax–Friedrichs scheme introduces stronger numerical dissipation through its averaging stencil. This enhances stability at the cost of increased smearing of the interval width over long integration times.*

5.2.3. Interval Lax–Wendroff Scheme

Lemma 3 (Consistency of the Interval Lax–Wendroff Scheme)**.** *The interval Lax–Wendroff scheme (27) is consistent with the interval advection Equation (13). Moreover, under the fixed mesh ratio $\Delta t/\Delta x = \lambda$, its local truncation error satisfies*

$$\|\overline{\mathcal{T}}_j^n\| = O(\Delta t^2 + \Delta x^2) \quad as \quad \Delta t, \Delta x \to 0. \tag{37}$$

Proof. The Lax–Wendroff scheme achieves second-order accuracy by incorporating additional terms that cancel the first-order error present in the simpler schemes. We outline the proof for the center component; the logarithmic radius component follows identically with velocity $\ln a_w$ and requires $\ln u_w \in C^4$.

For the classical Lax–Wendroff scheme applied to $v_t + cv_x = 0$, the key idea is to replace the time derivative v_{tt} in the Taylor expansion by spatial derivatives using the governing PDE:

$$v_{tt} = (v_t)_t = (-cv_x)_t = -c(v_t)_x = -c(-cv_x)_x = c^2 v_{xx}.$$

Substituting the exact solution and expanding to fourth order, the truncation error becomes

$$\begin{aligned}\mathcal{T}_{\mathrm{LW}} &= \frac{1}{\Delta t}\left(v + \Delta t\, v_t + \frac{\Delta t^2}{2} v_{tt} + \frac{\Delta t^3}{6} v_{ttt} + \frac{\Delta t^4}{24} v_{tttt} + \cdots\right) \\ &\quad - \frac{1}{\Delta t}\left(v + \Delta t\, cv_x - \frac{\Delta t^2}{2} c^2 v_{xx} - \frac{\Delta t \Delta x^2}{6} cv_{xxx} + \frac{\Delta t^2 \Delta x^2}{12} c^2 v_{xxxx} + \cdots\right) \\ &= \frac{\Delta t^2}{6}(v_{ttt} + c^3 v_{xxx}) + \frac{\Delta t^3}{24} v_{tttt} + \frac{\Delta x^2}{6} cv_{xxx} + O(\Delta t^4 + \Delta t^2 \Delta x^2 + \Delta x^4).\end{aligned} \tag{38}$$

The terms of order Δt^2 and Δx^2 cancel precisely because of the relation $v_{tt} = c^2 v_{xx}$ and the carefully chosen coefficients in the scheme. The remaining leading terms involve third and fourth derivatives. Under the smoothness assumption $v \in C^4$, these derivatives are bounded, giving $|\mathcal{T}_{\mathrm{LW}}| = O(\Delta t^2 + \Delta x^2)$.

For the center component u_c with velocity a_c, the second-order terms cancel after substituting $(u_c)_{tt} = a_c^2 (u_c)_{xx}$. The leading remainder involves third-order derivatives:

$$(\mathcal{T}_c)_j^n = \frac{\Delta t^2}{6}(u_c)_{ttt} - \frac{a_c \Delta x^2}{6}(u_c)_{xxx} + O(\Delta t^3 + \Delta t \Delta x^2 + \Delta x^3).$$

Using the advection equation to replace time derivatives $(u_c)_{ttt} = -a_c^3 (u_c)_{xxx}$, we rewrite the leading error in terms of the CFL number $\nu_c = |a_c|\Delta t/\Delta x$:

$$(\mathcal{T}_c)_j^n = \frac{a_c \Delta x^2}{6}\left(1 - \nu_c^2\right)(u_c)_{xxx} + O(\Delta t^3 + \Delta x^3),$$

which explicitly shows the dependence of the truncation error on the mesh ratio.

For the logarithmic-radius component $v = \ln u_w$ with velocity $b = \ln a_w$, the same fourth-order Taylor expansion and cancellation argument apply:

$$(\mathcal{T}_{\ln w})_j^n = \frac{\Delta t^2}{6} v_{ttt} - \frac{b \Delta x^2}{6} v_{xxx} + O(\Delta t^3 + \Delta t \Delta x^2 + \Delta x^3).$$

Substituting $v_{ttt} = -b^3 v_{xxx}$ and defining $\nu_w = |b|\Delta t/\Delta x$, the leading remainder becomes

$$(\mathcal{T}_{\ln w})_j^n = \frac{b \Delta x^2}{6}\left(1 - \nu_w^2\right) v_{xxx} + O(\Delta t^3 + \Delta x^3),$$

with second-order terms vanishing identically. Under the regularity assumption $v \in C^4$, the leading remainder is bounded, under a fixed mesh ratio, giving second-order accuracy for both components. Combining the component errors via the interval norm, we obtain the estimate (37). The higher regularity requirement C^4 (compared with C^2 for the first-order schemes) is essential: the Taylor expansion used in the cancellation argument requires bounded fourth derivatives to control the remainder terms. □

Remark 9. *The Lax–Wendroff scheme achieves second-order accuracy by canceling the leading error term. It is the preferred choice when high-fidelity preservation of both the center profile and the interval width is required for smooth solutions.*

5.3. Stability Analysis and the CFL Condition

We now analyze the stability of the proposed schemes using the von Neumann (Fourier) method. Under the periodic boundary conditions (13), any interval grid function can be expanded in Fourier modes. Because the interval norm decomposes orthogonally as shown in (30), the stability of the interval scheme is equivalent to the simultaneous stability of the center and logarithmic-radius component schemes.

Theorem 4 (Stability and CFL Condition)**.** *All three interval schemes—Upwind* (20)*, Lax–Friedrichs* (23)*, and Lax–Wendroff* (27)*—are stable in the discrete L_2 norm* (30) *under the CFL condition*

$$\nu := \max\left(|a_c|, |\ln a_w|\right)\frac{\Delta t}{\Delta x} \le 1. \tag{39}$$

Proof. We present the proof assuming $a_c > 0$ and $\ln a_w > 0$ for notational simplicity. For velocities of arbitrary sign, the upwind stencil is flipped accordingly and the velocities are replaced by their absolute values $|a_c|$ and $|\ln a_w|$. Since the modulus of the amplification factor depends only on the velocity magnitude rather than its sign, the CFL condition (39) remains unchanged and covers all sign combinations.

(1) **Upwind scheme.** Substituting the Fourier mode $\overline{U}_j^n = \langle \hat{U}_c^n e^{i\xi j \Delta x}; \exp(\hat{V}^n e^{i\xi j \Delta x})\rangle$ into (20) and projecting onto the center and radius components, we obtain the amplification factors

$$G_c(\xi) = 1 - a_c \frac{\Delta t}{\Delta x}(1 - e^{-i\xi\Delta x}), \qquad G_w(\xi) = 1 - \ln a_w \frac{\Delta t}{\Delta x}(1 - e^{-i\xi\Delta x}).$$

These are precisely the amplification factors of the classical first-order upwind scheme. A standard calculation gives

$$|G_c(\xi)|^2 = 1 - 2a_c \frac{\Delta t}{\Delta x}\left(1 - a_c \frac{\Delta t}{\Delta x}\right)(1 - \cos \xi \Delta x).$$

The condition $|G_c(\xi)| \leq 1$ for all ξ is, therefore, equivalent to $a_c \Delta t/\Delta x \leq 1$. Similarly, $|G_w(\xi)| \leq 1$ requires $|\ln a_w|\Delta t/\Delta x \leq 1$. Both conditions must hold simultaneously, leading to (39).

(2) **Lax–Friedrichs scheme.** For the classical Lax–Friedrichs scheme, the amplification factor is

$$G(\xi) = \cos \xi \Delta x - ic \frac{\Delta t}{\Delta x} \sin \xi \Delta x,$$

with $|G(\xi)|^2 = \cos^2 \xi \Delta x + c^2 (\Delta t/\Delta x)^2 \sin^2 \xi \Delta x$. The condition $|G(\xi)| \leq 1$ is equivalent to $|c|\Delta t/\Delta x \leq 1$. Applying this with $c = a_c$ and $c = \ln a_w$ again yields (39).

(3) **Lax–Wendroff scheme.** The amplification factor for the classical Lax–Wendroff scheme is

$$G(\xi) = 1 - ic \frac{\Delta t}{\Delta x} \sin \xi \Delta x - 2c^2 \frac{\Delta t^2}{\Delta x^2} \sin^2 \frac{\xi \Delta x}{2}.$$

Its squared modulus is

$$|G(\xi)|^2 = 1 - 4c^2 \frac{\Delta t^2}{\Delta x^2}\left(1 - c^2 \frac{\Delta t^2}{\Delta x^2}\right) \sin^4 \frac{\xi \Delta x}{2}.$$

The condition $|G(\xi)| \leq 1$ for all ξ is equivalent to $|c|\Delta t/\Delta x \leq 1$. Substituting $c = a_c$ and $c = \ln a_w$ yields (39) once again.

Having established that each component scheme is stable under (39), the stability of the interval scheme follows directly from the norm decomposition (30):

$$\|\overline{U}^n\|_{L_2}^2 = \|U_c^n\|_{L_2}^2 + \|\ln U_w^n\|_{L_2}^2 \leq \|U_c^0\|_{L_2}^2 + \|\ln U_w^0\|_{L_2}^2 = \|\overline{U}^0\|_{L_2}^2,$$

completing the proof. □

Remark 10. *The CFL condition (39) involves two velocities: the center advection speed a_c and the logarithmic radius speed $\ln a_w$. The more restrictive of the two determines the allowable time step. If $a_w = 1$, then $\ln a_w = 0$ and the condition reduces to the classical $|a_c|\Delta t/\Delta x \leq 1$. In practice, the time step should be chosen as large as possible subject to this condition to minimize numerical diffusion. When $\nu = 1$, the amplification factor has unit modulus and the schemes remain von Neumann stable (neutrally stable), with numerical dissipation vanishing entirely. For smooth initial data, the schemes reproduce exact translation along characteristics. The upwind and Lax–Friedrichs schemes are advected without dissipation at $\nu = 1$; the Lax–Wendroff scheme retains non-zero dispersion error, so $\nu < 1$ is recommended for general computations.*

5.4. Convergence Analysis

Under the CFL condition (39), the discrete evolution operators satisfy the energy estimate

$$\|\bar{U}^n\|_{L_2} \leq \|\bar{U}^0\|_{L_2}$$

for all $n \geq 0$, as established in Theorem 4. By the isometric isomorphism Φ, this contraction property extends directly to the interval Hilbert space $(\mathbb{R}_I, \|\cdot\|)$, so the family of evolution operators is uniformly bounded with respect to n and Δt. This uniform boundedness, together with the consistency results in Section 5.2, completes the hypotheses required by the Lax equivalence theorem.

Theorem 5 (Convergence of the Interval Schemes)**.** *Let $\overline{u}(x,t)$ be the exact solution of the interval advection Equation (13) with sufficiently smooth initial data. For any of the three interval schemes, under the fixed mesh ratio $\Delta t/\Delta x = \lambda$ and the CFL condition (39), the numerical solution $\overline{U}_j^n$ converges to $\overline{u}(x_j, t_n)$ in the discrete L_2 norm. Specifically, there exists a constant $C > 0$ independent of Δt and Δx, such that*

$$\|\overline{U}^n - \overline{u}(\cdot, t_n)\|_{L_2} \leq C\Delta x^p, \tag{40}$$

where $p = 1$ for the Upwind and Lax–Friedrichs schemes, and $p = 2$ for the Lax–Wendroff scheme.

Proof. The interval advection Equation (13) is linear with constant coefficients and is well-posed in the Hilbert space $(\mathbb{R}_\mathcal{I}, \|\cdot\|)$. The numerical schemes define linear evolution operators on the space of interval grid functions. Lemmas 1–3 establish that the schemes are consistent, with local truncation errors of order p as stated. Combined with the uniform boundedness of the evolution operators established above, Theorem 4 guarantees stability in the interval norm under the CFL condition (39). By the Lax equivalence theorem (see, e.g., [15]), consistency and stability imply convergence, and the global error is of the same order as the local truncation error. Under the fixed mesh ratio, $\Delta t^p + \Delta x^p$ reduces to $O(\Delta x^p)$, yielding (40). $\square$

Remark 11. *The convergence analysis illustrates a fundamental strength of the new interval calculus: the entire proof is conducted within the interval space $\mathbb{R}_\mathcal{I}$ using its intrinsic norm, without any need for endpoint tracking or switching-point logic. The decoupling into independent classical schemes is invoked only at the computational level, while the theoretical guarantees are obtained directly in the interval framework.*

6. Numerical Experiments

In this section, we present a comprehensive numerical study to validate the theoretical results established in Section 5 and to demonstrate the practical advantages of the proposed interval difference schemes. The experiments are organized as follows: Section 6.1 describes the common experimental setup, including the baseline gH-Upwind scheme used for comparison. Sections 6.2–6.6 then present the convergence test, CFL validation, width evolution comparison, decoupled propagation and interval envelope, and computational efficiency, respectively.

6.1. Experimental Setup

We consider the interval advection Equation (13) on the periodic spatial domain $x \in [0,1]$ ($L = 1$) with final time $T = 1.0$ unless otherwise specified. Two representative advection velocities are employed:

- Case A: $a_c = 1.0,\ a_w = 2.0 \quad (\ln a_w \approx 0.693 > 0)$;
- Case B: $a_c = 1.0,\ a_w = 0.5 \quad (\ln a_w \approx -0.693 < 0)$.

The initial condition is given in center-radius form by

$$\begin{aligned} &\overline{u}_0(x) = \langle u_{c,0}(x); u_{w,0}(x) \rangle, \\ &u_{c,0}(x) = A\sin(2\pi x), \quad u_{w,0}(x) = A(2 + \cos(2\pi x)), \end{aligned} \tag{41}$$

where the amplitude factor A is set to 1 for convergence and decoupling tests, and to 10 (resp. 5) for width evolution and stability tests to amplify the observable effects. The exact solution is obtained via the decoupled system (17) using the method of characteristics.

For the initial condition (41), the exact solution of the decoupled system (17) with periodic boundary conditions is given by the method of characteristics:

$$u_c(x,t) = u_{c,0}\big((x - a_c t) \bmod L\big), \qquad \ln u_w(x,t) = \ln u_{w,0}\big((x - \ln a_w \cdot t) \bmod L\big),$$

where $\bmod L$ denotes the periodic folding of the spatial argument into the domain $[0, L]$. Specifically, for any $y \in \mathbb{R}$, $y \bmod L$ is the unique value in $[0, L)$ such that $y - (y \bmod L) \in L\mathbb{Z}$. The radius component and interval endpoints are then reconstructed as

$$u_w(x,t) = \exp\big(\ln u_w(x,t)\big), \qquad u_l(x,t) = u_c(x,t) - u_w(x,t), \qquad u_r(x,t) = u_c(x,t) + u_w(x,t).$$

The numerical errors reported in Section 6.2 are computed using the discrete L_2 norm (30) evaluated at the grid points $x_j = j\Delta x$.

The numerical schemes under investigation are as follows:

(1) IU—Interval Upwind scheme (20);
(2) ILF—Interval Lax–Friedrichs scheme (23);
(3) ILW—Interval Lax–Wendroff scheme (27).

To benchmark the performance of these new interval schemes, we also implement as a baseline the conventional upwind scheme based on Moore's interval arithmetic [1] and the generalized Hukuhara (gH) difference introduced by Stefanini and Bede [3]. The gH-Upwind scheme for (13) reads

$$\overline{U}_j^{n+1} = \overline{U}_j^n \ominus_{gH} \left(\overline{a} \otimes \frac{\Delta t}{\Delta x} \otimes \left(\overline{U}_j^n \ominus_{gH} \overline{U}_{j-1}^n\right)\right), \tag{42}$$

where $\ominus_{gH}$ is the gH-difference defined in (6) and $\otimes$ denotes Moore's interval multiplication, which is implemented via the four endpoint products as described in [1]. In contrast to the decoupled center-radius updates of the new interval schemes, the gH-Upwind scheme requires explicit tracking of interval endpoints and involves min / max operations at every grid point and time step.

All algorithms are implemented in Python 3.12.4 using `numpy` for array operations. The discrete L_2 error is computed according to (30). The mesh ratio $\Delta t/\Delta x$ is held fixed during convergence tests, and the CFL number is defined as $\nu = \max(|a_c|, |\ln a_w|)\Delta t/\Delta x$.

6.2. Convergence Order Verification

We first examine the convergence rates of the IU, ILF, and ILW schemes for Case A. The simulation is run on a sequence of grids with $N_x = 40, 80, 160, 320, 640$ and a fixed CFL number $\nu = 0.8$. The L_2 error at $T = 1.0$ is recorded for each scheme.

Figure 1 displays the log–log plot of the error against the spatial step size Δx. The IU and ILF schemes exhibit first-order convergence, as their error curves are nearly parallel to the reference slope of 1. The ILW scheme achieves second-order accuracy, closely following the slope-2 reference line. These numerical orders are in full agreement with the theoretical predictions of Lemmas 1–3, confirming that the decoupled formulation correctly inherits the convergence properties of the underlying classical schemes.

To quantitatively validate the convergence behavior and provide detailed error statistics, we summarize the numerical results in Table 1. As the mesh is refined, the observed convergence orders gradually approach the theoretical values: first order for the IU and ILF schemes, and second order for the ILW scheme. This quantitative evidence is fully consistent with the trends shown in Figure 1 and the theoretical analysis in Section 5.

6.3. CFL Condition and Stability

To validate the stability condition (39), we perform simulations for Case A with a fixed spatial grid $N_x = 200$ and vary the CFL number ν from 0.2 to 1.4 in increments of 0.2. The final time is extended to $T = 2.0$ to allow potential instabilities to fully develop. For each run, the maximum L_2 error over the last 20% of the time steps is recorded.

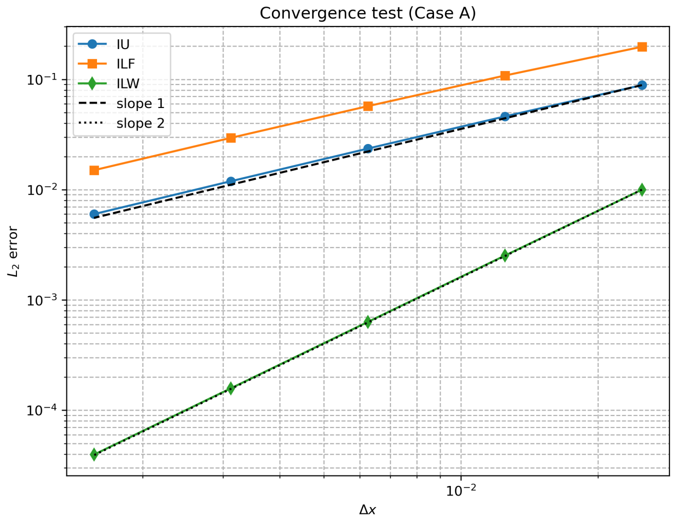

Figure 1. Double logarithmic plot of the L_2 error versus Δx for the interval schemes.

Table 1. Convergence study for the IU, ILF, and ILW schemes at $T = 1.0$ with $\nu = 0.8$ (Case A). Errors are measured in the discrete L_2 norm.

Scheme	N_x	Δx	Δt	N_t	$E\ (u_c)$	$E\ (\ln u_w)$	E_{total}	Order (u_c)	Order $(\ln u_w)$
IU	40	0.0250	0.020000	50	6.65×10^{-2}	5.88×10^{-2}	8.88×10^{-2}	–	–
	80	0.0125	0.010000	100	3.41×10^{-2}	3.12×10^{-2}	4.62×10^{-2}	0.97	0.92
	160	0.0063	0.005000	200	1.72×10^{-2}	1.61×10^{-2}	2.36×10^{-2}	0.98	0.95
	320	0.0031	0.002500	400	8.67×10^{-3}	8.20×10^{-3}	1.19×10^{-2}	0.99	0.97
	640	0.0016	0.001250	800	4.35×10^{-3}	4.14×10^{-3}	6.00×10^{-3}	1.00	0.99
ILF	40	0.0250	0.020000	50	1.41×10^{-1}	1.39×10^{-1}	1.98×10^{-1}	–	–
	80	0.0125	0.010000	100	7.43×10^{-2}	7.90×10^{-2}	1.08×10^{-1}	0.92	0.81
	160	0.0063	0.005000	200	3.82×10^{-2}	4.27×10^{-2}	5.72×10^{-2}	0.96	0.89
	320	0.0031	0.002500	400	1.94×10^{-2}	2.23×10^{-2}	2.95×10^{-2}	0.98	0.94
	640	0.0016	0.001250	800	9.75×10^{-3}	1.14×10^{-2}	1.50×10^{-2}	0.99	0.97
ILW	40	0.0250	0.020000	50	6.56×10^{-3}	7.55×10^{-3}	1.00×10^{-2}	–	–
	80	0.0125	0.010000	100	1.64×10^{-3}	1.92×10^{-3}	2.53×10^{-3}	2.00	1.98
	160	0.0063	0.005000	200	4.11×10^{-4}	4.81×10^{-4}	6.32×10^{-4}	2.00	2.00
	320	0.0031	0.002500	400	1.03×10^{-4}	1.20×10^{-4}	1.58×10^{-4}	2.00	2.00
	640	0.0016	0.001250	800	2.57×10^{-5}	3.01×10^{-5}	3.95×10^{-5}	2.00	2.00

Figure 2 presents the results on a semi-logarithmic scale. For $\nu \leq 1.0$, the error remains bounded at approximately 10^{-2}, which is consistent with the truncation error of the first-order schemes. As soon as ν exceeds unity, the error grows explosively, reaching 10^{100} and triggering floating-point overflow. This sharp threshold perfectly matches the theoretical CFL condition $\max(|a_c|, |\ln a_w|)\Delta t/\Delta x \leq 1$ derived in Theorem 4, thereby confirming the stability analysis.

6.4. Evolution of Interval Width: Comparison with gH-Upwind

A well-known drawback of traditional interval arithmetic is the artificial growth of interval width due to the accumulation of overestimation. To illustrate the superiority of the new interval calculus in this regard, we compare the maximum interval width produced by the IU scheme and the gH-Upwind scheme (42). The parameters correspond to Case A with an initial amplitude $A = 10$. The simulation is run up to $T = 2.0$ on a grid with $N_x = 200$ and $\nu = 0.8$.

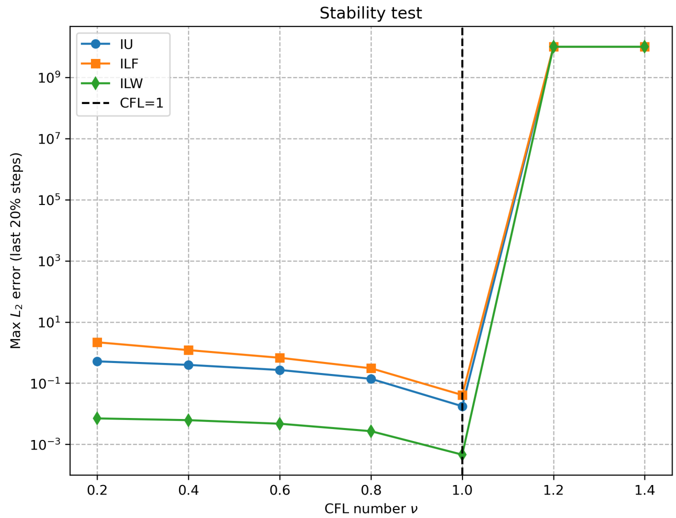

Figure 2. Semi-log plot of the maximum L_2 error versus CFL number ν.

Figure 3 depicts the temporal evolution of the maximum width in both linear (a) and logarithmic (b) scales. Under the new Upwind scheme, the width remains nearly constant, decreasing only slightly from 60.0 to approximately 58.8 due to the numerical dissipation inherent to first-order upwinding. In stark contrast, the gH-Upwind scheme suffers from an immediate and unbounded growth: the width escalates from 60 to 1.26×10^{17} at $t = 0.2$, and exceeds 10^{100} by $t = 1.0$, at which point the simulation is terminated. This explosive behavior vividly demonstrates the overestimation phenomenon of conventional interval methods and highlights the robustness of the new interval arithmetic, which inherently preserves the linear structure of the advection equation.

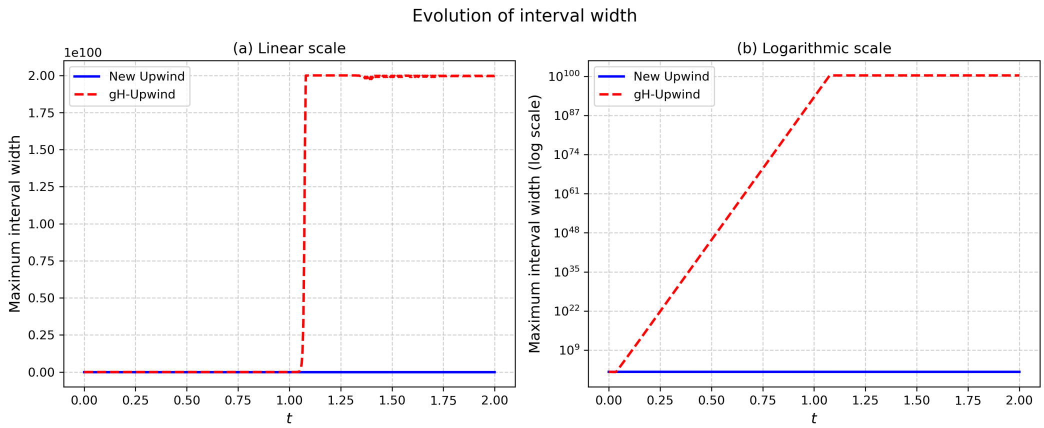

Figure 3. Temporal evolution of the maximum interval width: (**a**) linear scale, (**b**) logarithmic scale.

6.5. Decoupled Propagation and Interval Envelope

The decoupling property (17) is visualized in Figure 4 for Case B ($a_c = 1.0, a_w = 0.5$). The ILW scheme is employed with $N_x = 400$ and $\nu = 0.8$. The left panel (a) shows the center component u_c, while the right panel (b) shows the logarithmic radius $\ln u_w$. At $T = 1.0$, the center profile has shifted rightward by approximately $a_c T = 1.0$, whereas the logarithmic radius has shifted leftward by $|\ln a_w| T \approx 0.693$. The numerical solutions (solid lines) are virtually indistinguishable from the exact solutions (dashed lines), confirming both the decoupled propagation and the high accuracy of the ILW scheme.

To further illustrate the interval-valued nature of the solution, Figure 5 displays the envelope of the interval solution at $T = 1.0$ for Case A with an amplified initial condition ($A = 10$). The upper bound u_r (red solid) and lower bound u_l (blue dashed) are smooth and non-intersecting, and the shaded region between them represents the uncertainty range. The absence of endpoint crossings or artificial width oscillations underscores another practical advantage of the new interval calculus: the natural preservation of interval endpoint ordering eliminates the need for switching-point logic that plagues gH-based schemes.

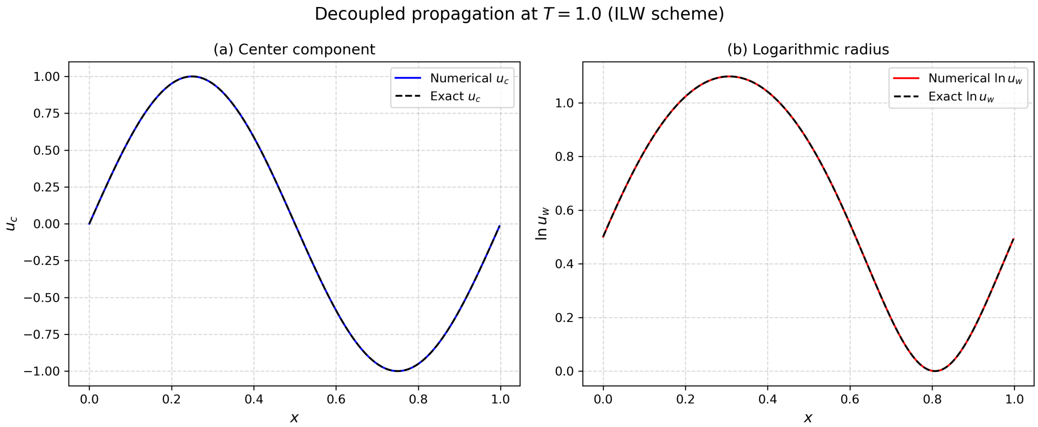

Figure 4. Decoupled propagation of center and logarithmic radius components at $T = 1.0$.

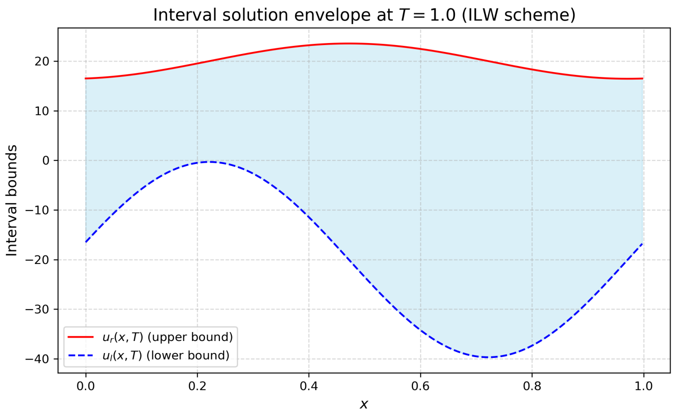

Figure 5. Interval solution envelope at $T = 1.0$.

6.6. Computational Efficiency

Finally, we assess the computational efficiency of the proposed schemes. Table 2 reports the average CPU time per time step for a fine grid of $N_x = 2000$ points, measured over 100 time steps and averaged over 5 independent runs.

All numerical experiments were performed on a workstation equipped with an Intel Core i5-8250U CPU (manufactured by Intel Corporation, Santa Clara, CA, USA; 4 cores, 1.80 GHz) and 8 GB RAM, running the Windows 11 operating system (developed by Microsoft Corporation, Redmond, WA, USA). The code was implemented in Python 3.12.4 with NumPy 1.26.4 linked against Intel MKL 2023.1, utilizing all available cores via multithreading. Computations use IEEE 754 double precision (float64) with hardware acceleration via SSE, AVX2, and FMA3. No explicit vectorization beyond NumPy's native operations was employed.

Runtime measurements were recorded using `time.perf_counter()` with a 10-step warm-up. All reported times are averaged over five independent runs, with standard deviations included in Table 2.

The IU scheme is the fastest, as it involves the fewest floating-point operations. The ILF and ILW schemes are slightly more expensive due to the additional stencil computations, while the gH-Upwind scheme exhibits a comparable cost to ILF. However, as demonstrated in Section 6.4, the gH scheme becomes numerically unstable and produces meaningless results beyond very short integration times, whereas the new interval schemes remain robust and accurate over arbitrarily long simulations. Moreover, the new schemes require no case-by-case switching logic, leading to a simpler and more maintainable implementation. Consequently, the new interval calculus offers decisive advantages in both reliability and long-time predictive capability.

Table 2. Average CPU time per time step (in milliseconds).

Scheme	Time/Step (ms)	Std (ms)
IU	0.0678	0.0026
ILF	0.1650	0.0088
ILW	0.1787	0.0219
gH	0.1505	0.0098

7. Conclusions

In this paper, we have developed and rigorously analyzed a family of finite difference schemes for the interval advection equation within the newly established interval calculus of Liu et al. [7]. By exploiting the center-radius representation and the fundamental decoupling property of the new interval derivative, we constructed interval analogues of the classical Upwind, Lax–Friedrichs, and Lax–Wendroff schemes. Each scheme was expressed both in a compact interval form, highlighting its algebraic closure within the interval space $\mathbb{R}_{\mathcal{I}}$, and in a component-wise multiplicative form that reveals a clean separation into classical advection schemes for the center and logarithmic radius components.

A comprehensive theoretical analysis was carried out directly in the interval space using the intrinsic norm $\|\cdot\|$ and the isometric isomorphism $\Phi : \mathbb{R}_{\mathcal{I}} \to \mathbb{R}^2$. We proved the consistency of all three schemes and derived their local truncation errors: first-order for the Upwind and Lax–Friedrichs schemes, and second-order for the Lax–Wendroff scheme. Stability was analyzed via the von Neumann method, leading to a unified CFL condition $\max(|a_c|, |\ln a_w|)\Delta t/\Delta x \leq 1$, in which the logarithmic velocity $\ln a_w$ emerges naturally from the multiplicative structure of the new interval arithmetic. Convergence was then established through the Lax equivalence theorem.

Extensive numerical experiments were conducted to validate the theoretical findings and to demonstrate the practical advantages of the proposed schemes. The results confirmed that

(1) The IU and ILF schemes achieve first-order convergence, while the ILW scheme attains second-order accuracy, in full agreement with the theoretical predictions.
(2) The CFL condition is sharp; violations lead to immediate and explosive error growth.
(3) The new interval schemes maintain a nearly constant interval width throughout long-time simulations, in stark contrast to the gH-based Upwind scheme (42), which suffers from unbounded width growth due to the overestimation inherent in traditional interval arithmetic.
(4) The decoupled propagation of the center and logarithmic radius components is accurately captured, and the interval solution envelope remains smooth and non-intersecting without any need for switching-point logic.
(5) The computational efficiency of the new schemes is comparable to that of the gH-based scheme, with the decisive added benefit of unconditional long-time stability and a simpler, switching-free implementation.

The main novel contributions of this work are summarized as follows:

(1) Three classical finite-difference schemes are rigorously extended to the interval advection equation under the new interval calculus, leveraging the exact center-radius decoupling property for algebraic closure.
(2) Complete consistency, stability and convergence analyses are established directly in the interval norm, with an explicit unified CFL condition matching the accuracy orders of deterministic schemes.
(3) The proposed schemes inherently eliminate artificial interval-width growth and switching-point complexities, enabling stable long-time simulations unavailable to traditional gH-based methods.

The present work demonstrates that the new interval calculus provides an elegant and powerful framework for the numerical solution of interval partial differential equations. The decoupling of center and radius dynamics not only simplifies the construction and analysis of numerical schemes but also eliminates the artificial width inflation and switching-point complexity that plague traditional interval methods. These advantages make the proposed approach particularly attractive for uncertainty quantification in advection-dominated problems arising in fluid dynamics, environmental modeling, and engineering applications.

Several promising directions for further research extend from this work:

(1) Extension of the proposed schemes to nonlinear interval advection equations and systems of interval conservation laws, to broaden the scope of applicability.
(2) Development of higher-order interval schemes, such as essentially non-oscillatory (ENO) or weighted ENO (WENO) methods, to further enhance accuracy while preserving the robust width-control properties observed here.
(3) Application of the new interval calculus to other classes of PDEs, including diffusion equations and wave equations, as a natural next step for the framework.
(4) Integration of adaptive mesh refinement techniques with the interval framework, to achieve greater computational efficiency for problems with localized uncertainty features.

We hope that this work will stimulate further investigations into the numerical analysis of interval PDEs within the new interval calculus and contribute to the broader adoption of rigorous uncertainty quantification methods in scientific computing.

Author Contributions: Conceptualization, J.W. and G.Y.; methodology, J.W. and W.L.; software, J.W.; validation, J.W. and A.M.; formal analysis, J.W. and W.L.; investigation, J.W. and A.M.; resources, G.Y. and G.A.; data curation, J.W.; writing—original draft preparation, J.W.; writing—review and editing, G.Y., W.L., A.M. and G.A.; visualization, J.W.; supervision, G.Y. and W.L.; project administration, A.M.; funding acquisition, G.A. All authors have read and agreed to the published version of the manuscript.

Funding: This research was supported by Princess Nourah bint Abdulrahman University Researchers Supporting Project number (PNURSP2026R45), Princess Nourah bint Abdulrahman University, Riyadh, Saudi Arabia.

Data Availability Statement: The data presented in this study are contained within the article.

Acknowledgments: This research was supported by Princess Nourah bint Abdulrahman University Researchers Supporting Project number (PNURSP2026R45), Princess Nourah bint Abdulrahman University, Riyadh, Saudi Arabia.

Conflicts of Interest: The authors declare no conflict of interest.

References

1. Moore, R.E. *Interval Analysis*; Prentice-Hall: Englewood Cliffs, NJ, USA, 1966.

2. Hansen, E.; Walster, G.W. *Global Optimization Using Interval Analysis*, 2nd ed.; Marcel Dekker: New York, NY, USA, 2004.
3. Stefanini, L.; Bede, B. Generalized Hukuhara differentiability of interval-valued functions and interval differential equations. *Nonlinear Anal.* **2009**, *71*, 1311–1328. [CrossRef]
4. Malinowski, M.T. Interval Cauchy problem with a second type Hukuhara derivative. *Inf. Sci.* **2012**, *213*, 94–105. [CrossRef]
5. Jaulin, L.; Kieffer, M.; Didrit, O.; Walter, É. *Applied Interval Analysis*; Springer: London, UK, 2001.
6. Sanchez, L.; Costa, N.; Couso, I.; Strauss, O. Integrating imprecise data in generative models using interval-valued variational autoencoders. *Inf. Fusion* **2025**, *114*, 102659. [CrossRef]
7. Liu, W.; Ali, M.A.; An, Y. New interval calculus with application to interval differential equations. *arXiv* **2025**, arXiv:2511.21696.
8. Grossman, M.; Katz, R. *Non-Newtonian Calculus*; Lee Press: Pigeon Cove, MA, USA, 1972.
9. Bashirov, A.E.; Kurpınar, E.M.; Özyapıcı, A. Multiplicative calculus and its applications. *J. Math. Anal. Appl.* **2008**, *337*, 36–48. [CrossRef]
10. Yazıcı, M.; Selvitopi, H. Numerical methods for the multiplicative partial differential equations. *Open Math.* **2017**, *15*, 1344–1350. [CrossRef]
11. Cubillos, M. Modelling wave propagation without sampling restrictions using the multiplicative calculus I: Theoretical considerations. *arXiv* **2018**, arXiv:1801.03402.
12. Riza, M.; Özyapici, A.; Misirli, E. Multiplicative finite difference methods. *Q. Appl. Math.* **2009**, *67*, 745–754. [CrossRef]
13. Aniszewska, D. Multiplicative Runge-Kutta methods. *Nonlinear Dyn.* **2007**, *50*, 265–272. [CrossRef]
14. Misirli, E.; Gurefe, Y. Multiplicative Adams Bashforth-Moulton methods. *Numer. Algorithms* **2011**, *57*, 425–439. [CrossRef]
15. Strikwerda, J.C. *Finite Difference Schemes and Partial Differential Equations*, 2nd ed.; SIAM: Philadelphia, PA, USA, 2004.

Disclaimer/Publisher's Note: The statements, opinions and data contained in all publications are solely those of the individual author(s) and contributor(s) and not of MDPI and/or the editor(s). MDPI and/or the editor(s) disclaim responsibility for any injury to people or property resulting from any ideas, methods, instructions or products referred to in the content.